



HAL
open science

The coordinated population redistribution between *Bacillus subtilis* submerged biofilm and liquid-air pellicle

Pilar Sanchez-Vizueté, Yasmine Dergham, Arnaud Bridier, Julien Deschamps, Etienne Dervyn, Kassem Hamze, Stéphane Aymerich, Dominique D. Le Coq, Romain Briandet

► To cite this version:

Pilar Sanchez-Vizueté, Yasmine Dergham, Arnaud Bridier, Julien Deschamps, Etienne Dervyn, et al.. The coordinated population redistribution between *Bacillus subtilis* submerged biofilm and liquid-air pellicle. *Biofilm*, 2022, 4, pp.100065. 10.1016/j.biofm.2021.100065 . hal-03501177

HAL Id: hal-03501177

<https://hal.inrae.fr/hal-03501177>

Submitted on 1 Mar 2022

HAL is a multi-disciplinary open access archive for the deposit and dissemination of scientific research documents, whether they are published or not. The documents may come from teaching and research institutions in France or abroad, or from public or private research centers.

L'archive ouverte pluridisciplinaire **HAL**, est destinée au dépôt et à la diffusion de documents scientifiques de niveau recherche, publiés ou non, émanant des établissements d'enseignement et de recherche français ou étrangers, des laboratoires publics ou privés.



Distributed under a Creative Commons Attribution - NonCommercial - NoDerivatives 4.0 International License



The coordinated population redistribution between *Bacillus subtilis* submerged biofilm and liquid-air pellicle[☆]

Pilar Sanchez-Vizueté^{a,1}, Yasmine Dergham^{a,b}, Arnaud Bridier^c, Julien Deschamps^a, Etienne Dervyn^a, Kassem Hamze^b, Stéphane Aymerich^a, Dominique Le Coq^{a,d}, Romain Briandet^{a,*}

^a Université Paris-Saclay, INRAE, AgroParisTech, Micalis Institute, 78350, Jouy-en-Josas, France

^b Faculty of Science, Lebanese University, 1003, Beirut, Lebanon

^c Fougères Laboratory, Antibiotics, Biocides, Residues and Resistance Unit, Anses, 35300, Fougères, France

^d Université Paris-Saclay, Centre National de la Recherche Scientifique (CNRS), INRAE, AgroParisTech, Micalis Institute, 78350, Jouy-en-Josas, France

ARTICLE INFO

Keywords:

Bacillus subtilis
Biofilm
Pellicle
4D-CLSM
Motility
Oxygen
Metabolism

ABSTRACT

Bacillus subtilis is a widely used bacterial model to decipher biofilm formation, genetic determinants and their regulation. For several years, studies were conducted on colonies or pellicles formed at the interface with air, but more recent works showed that non-domesticated strains were able to form thick and structured biofilms on submerged surfaces. Taking advantage of time-lapse confocal laser scanning microscopy, we monitored bacterial colonization on the surface and observed an unexpected biphasic submerged biofilm development. Cells adhering to the surface firstly form elongated chains before being suddenly fragmented and released as free motile cells in the medium. This switching coincided with an oxygen depletion in the well which preceded the formation of the pellicle at the liquid-air interface. Residual bacteria still associated with the solid surface at the bottom of the well started to express matrix genes under anaerobic metabolism to build the typical biofilm protruding structures.

1. Introduction

In their natural habitat, bacteria mostly live in biofilms, associated with surfaces and embedded in a complex mixture of exopolymers [1]. These structures provide to their inhabitants a protective environment in which they can resist harsh conditions such as desiccation, nutrients starvation or the action of toxic compounds [2]. Microbial biofilms can be considered useful since they are involved in natural biogeochemical cycles and increasingly used in biotechnologies for wastewater treatments or the production of green energies [3]. However, biofilms also facilitate pathogen persistence despite antimicrobial treatments and thus have a severe negative impact in human health being involved in up to 80% of chronic and recurrent infections [4].

These infectious concerns have driven the international research efforts for more than 30 years to unravel the mechanisms of biofilm

formation and their control [5–7]. Most of the pioneer studies in this field have been carried out with axenic biofilms of pathogenic strains, such as *Pseudomonas aeruginosa*, grown in flow-cells and observed by *in situ* confocal imaging [8]. In the early 2000s, *Bacillus subtilis* emerged as a model of Gram-positive bacteria for the dissection of the genetic determinants of biofilm formation and their regulation [9,10]. Most of these studies used the strain NCIB3610, that has been shown to form spatially organized multicellular structures *i.e.* colony on agar, floating pellicle at the liquid-air interface, and submerged biofilm at the solid-liquid interface [9,11–13]. These experimental models have then been successfully used to dissect the complexity of *B. subtilis* multicellularity and their genetic circuits to identify the regulators controlling biofilm development, maturation and dispersion (e.g. Spo0A, SinR, SinI, AbrB, SlrR or SigB) [12,14–19]. In response to external signals, individual motile cells switch to sessile chains by inactivating expression of

[☆] ‘Given his role as Editor, Romain Briandet had no involvement in the peer review of this article and has no access to information regarding its peer review. Full responsibility for the editorial process for this article was delegated to Ákos T. Kovács’.

* Corresponding author.

E-mail address: romain.briandet@inrae.fr (R. Briandet).

¹ present address pilarsanzv@gmail.com

<https://doi.org/10.1016/j.biofilm.2021.100065>

Received 31 August 2021; Received in revised form 9 December 2021; Accepted 14 December 2021

Available online 18 December 2021

2590-2075/© 2021 The Author(s).

Published by Elsevier B.V. This is an open access article under the CC BY-NC-ND license

(<http://creativecommons.org/licenses/by-nc-nd/4.0/>).

the motility genes (*hag*, encoding the principal flagellar protein and *lytABC* and *lytF*, encoding the autolysins responsible of cell separation) and by activation of the matrix production genes [20–22]. This matrix of *B. subtilis* biofilms is essentially composed of the polysaccharides synthesized by the products of the 15-genes operon *epsA-O* (*eps* operon), the amyloid-like protein TasA, synthesized from the *tapA-sipW-tasA* operon, and the amphiphilic protein BslA [23–27].

Focusing on non-domesticated *B. subtilis* strains isolated from food or from medical environments, we showed that some strains, especially the NDmed strain isolated from an endoscope washer-disinfector, were able to form thick and structured biofilms on submerged surfaces [28]. Moreover, NDmed was able to protect *Staphylococcus aureus* from biocide action in a submerged mixed-species biofilm [29]. The gene *ypqP* (renamed *spsM* [30]) likely involved in the synthesis of polysaccharide, is inactivated in both the model strain NCIB3610 and the lab strain 168, and was identified as being responsible for these features of NDmed submerged biofilms [13].

These works point out the importance of the submerged biofilm as a model of growth in the study of *B. subtilis* social behavior. Moreover *B. subtilis* submerged biofilms are also considered to be representative of other *B. subtilis* natural habitats such as soil and plant roots surface [31, 32]. Nevertheless, little is still known about the genetic pathways involved in the formation of *B. subtilis* submerged biofilms [28,33,34].

To better understand the molecular strategies that bacteria undergo to build biofilms, we used 4D confocal laser scanning imaging (4D-CLSM) to visualize, *in situ*, in time-lapse and at cell level, the biofilm structural dynamics. By this approach, we have discovered that the transition from sessile cells to a highly structured biofilm of *B. subtilis* on the submerged level involves an unexpected sudden and coordinated fragmentation of the sessile population to a motile one. The latter event has been shown to be closely connected with the pellicle formation at the liquid-air interface and with transition from aerobic to anaerobic metabolisms. This work points out sophisticated programs of cellular specialization and cell-cell communication within the microbial community.

2. Materials and methods

2.1. Bacterial strains and growth conditions

The strains used during this study are listed in Table 1. *B. subtilis* NDmed derivative strains were obtained by transformation with chromosomal DNA of various strains to introduce the corresponding suitable reporter fusion. Extraction of chromosomal DNA and transformation of *B. subtilis* were performed as described previously [34]; transformants were selected on Luria-Bertani (LB, Sigma, France) plates supplemented with appropriate antibiotics at the following concentrations: spectinomycin (spec), 100 µg/mL; chloramphenicol (cm), 5 µg/mL kanamycin (kan), 8 µg/mL. The *B. subtilis* strain GM2938 expressing mCherry was obtained by transforming for spectinomycin resistance strain BSB168, a *trp* + derivative of the reference strain 168 Marburg [37] with plasmid pIC630. This results in the integration by a double crossing over into the chromosomal *amyE* locus of the *mCherry* gene placed under the control of the *Phyperspank* promoter, an isopropyl β-D-1-thiogalactopyranoside (IPTG)-inducible promoter derived from the *Escherichia coli lac* operon. Plasmid pIC630 was constructed by placing the *mCherry* gene (codon-optimized for *B. subtilis*) under the control of *Phyperspank* through cloning into pDR111 of a *HindIII-SphI* restriction fragment obtained from a PCR on plasmid pDR201 with primers DC014 (5'-CCCAAGCTTACATAAGGAGGAAGCTACTATG-3') and DC015 (5'-ACATGCATGCTTATTTGTATAATTC-3') (both pDR111 and pDR201 are kind gifts from D. Rudner, Harvard Medical School). A similar IPTG-inducible fusion of the *gfpmut2* gene under the control of the *Phyperspank* promoter was introduced into NDmed to give the *B. subtilis* strain NDmed-GFP expressing GFPmut2. The transcriptional fusions of the *fnr* or *gapB* promoter with *gfpmut3* were constructed within the pBasysBioII plasmid

Table 1
Strains used in this study.

Strain	Relevant genotype or isolation source	Reference or construction ^a
<i>B. subtilis</i> NDmed	Undomesticated, isolated from endoscope washer-disinfectors	[35]
<i>B. subtilis</i> NDmed-GFP	NDmed <i>amyE::Phyperspank-gfpmut2</i> (spec)	[29]
<i>B. subtilis</i> GM2938	BSB168 <i>amyE::Phyperspank-mCherry</i> (spec)	This work
<i>B. subtilis</i> NDmed-mCherry	NDmed <i>amyE::Phyperspank-mCherry</i> (spec)	TF NDmed/DNA GM2938
<i>B. subtilis</i> TMN547	NCIB3610 <i>amyE::Phag-gfp</i> (cm) <i>sacA::PtapA-mKate2</i> (kan)	[36]
<i>B. subtilis</i> NDmed 547	NDmed <i>amyE::Phag-gfp</i> (cm) <i>sacA::PtapA-mKate2</i> (kan)	TF NDmed/DNA TMN547
<i>B. subtilis</i> BBA9006	BSB168 <i>PgapB-gfpmut3</i> (spec)	[37]
<i>B. subtilis</i> GM3378	NDmed <i>PgapB-gfpmut3</i> (spec)	TF NDmed/DNA BBA9006
<i>B. subtilis</i> BBA0184	BSB168 <i>Pfnr-gfpmut3</i> (spec)	[38]
<i>B. subtilis</i> GM3361	NDmed <i>Pfnr-gfpmut3</i> (spec)	TF NDmed/DNA BBA0184
<i>B. subtilis</i> 168	<i>trpC2</i> (Domesticated strain)	<i>Bacillus</i> genetics Stock Center
<i>B. subtilis</i> BSB168	<i>trp</i> + derivative of 168	[37]
<i>B. subtilis</i> NCIB3610	Less domesticated strain	[9]
<i>B. subtilis</i> NDfood	Isolated from a dairy product	[28]
<i>B. subtilis</i> BSn5	Isolated from a plant	[39]
<i>B. subtilis</i> BSP1	Isolated from poultry	[40]
<i>B. cereus</i> 407		[41]
<i>B. licheniformis</i> LMG7559	Isolated from flour	[42]
<i>B. amyloliquefaciens</i> 20P6	Isolated from lettuce	This work

^a TF NDmed/DNA stands for transformation of NDmed by chromosomal DNA of indicated strains.

using ligation-independent cloning prior to integration into the chromosome of BSB168 in a non-mutagenic manner, resulting in strains BBA0184 and BBA9006, respectively [37,38]. Bacterial stock cultures were kept at –20°C in Tryptone Soy Broth (TSB, bioMerieux, France) containing 20% (vol/vol) glycerol. Prior to each experiment, frozen cells were sub-cultured twice in TSB at 30°C. The final overnight culture was used as an inoculum for the growth of biofilms.

2.2. Biofilm development in 96 well microplates

Submerged biofilms were grown on the surface of polystyrene 96-well microtiter plates with a µclear® base (Greiner Bio-one, France) enabling high-resolution fluorescence imaging [43]. 200 µL of an overnight culture in TSB (adjusted to an OD 600 nm of 0.02) were added in each well. The microtiter plate was then incubated at 30°C for 90 min to allow the bacteria to adhere to the bottom of the wells. Wells were then rinsed with TSB to eliminate non-adherent bacteria and refilled with 200 µL of sterile TSB. When appropriate, the medium was supplemented with 200 µM IPTG to induce the expression of the fluorescent reporters GFP or mCherry from the *Phyperspank* promoter. The vital stain FM4-64 (Invitrogen), added to the medium at a final concentration of 1 µg/mL, was used to label bacteria membranes when appropriate.

In order to acquire high resolution images of pellicle (Fig. 3B), floating biofilms grown in a 12-well microplate (Greiner bio-one, Germany) were detached by a tip from the sides of the well and placed on a slide to be observed under confocal microscopy.

2.3. 4D-CLSM

After the initial adhesion and washing steps, the 96 well microtiter plate was mounted on the motorized stage of a Leica SP8 AOBIS inverter confocal laser scanning microscope (CLSM, LEICA Microsystems, Germany) at the MIMA2 platform (www6.jouy.inra.fr/mima2_eng/).

Temperature was maintained at 30°C during all experiments. 4D (xyzt) acquisitions were performed with the following parameters: images of $246 \times 246 \mu\text{m}$ were acquired at 600 Hz using a $63 \times /1.2$ N.A. with a z-step of $1 \mu\text{m}$ and a thickness of $120 \mu\text{m}$ at intervals of 15 min. To detect GFP, an argon laser at 488 nm set at 10% of the maximal intensity was used, and the emitted fluorescence was collected in the range 495–550 nm using hybrid detectors (HyD LEICA Microsystems, Germany). To detect the red fluorescence of mKate2 or FM4-64, a 561 nm helium-neon laser set at 25% and 2% of the maximal intensity respectively was used, and fluorescence was collected in the range 590–720 nm and 605–705 nm respectively, using hybrid detectors.

To visualize simultaneously submerged biofilm and liquid-air pellicle dynamic (Fig. 1), the control software was set to take xyzt series of 1.5×1.5 mm images scanned at 600 Hz using a low-resolution long range $10 \times /0.3$ N.A. air objective with a z-step of $5 \mu\text{m}$ and a thickness of 4.5 mm at intervals of 60 min. To detect mCherry emitted fluorescence, a 561 nm helium-neon laser set at 20% of the maximal intensity was used, and fluorescence was collected in the range 580–700 nm using hybrid detectors. High resolution imaging of 24h culture biofilms (Fig. 3B) was obtained with a HCX APO L U–V–I 40x/0.80 WATER objective lens in well filled only 100 μL of growth media to reduce the distance between both interfaces.

2.4. CLSM image analysis

Projections of the biofilm structural dynamic were constructed from xyzt images series using IMARIS 9.3 (Bitplane, Switzerland). Individual cell length and numbers were extracted from 4D-CLSM with the ImageJ (v1.53) particle analysis function. Space-time kymographs were constructed with the BiofilmQ visualisation toolbox [44]. Local density color code was calculated with BiofilmQ after Otsu segmentation and visualized with Paraview 5.9 [45].

2.5. Temporal transcriptome analysis

Biofilms were grown as previously explained. Briefly, 200 μL of an overnight culture of NDmed in TSB (adjusted to an OD 600 nm of 0.02) were added in each well. The microtiter plate was then incubated at 30°C for 90 min to allow the bacteria to adhere to the bottom of the wells. Wells were then rinsed with TSB to eliminate non-adherent bacteria and refilled with 200 μL of sterile TSB. For each time point (1h, 3h, 4h, 5h, 7h, 24h and 48h) 96-well plates were prepared. At each time point, the content of the wells was recovered and put into contact with the same volume of killing buffer [46].

Then, RNA was extracted following the method described by [46]. The RNA concentration was measured using Nanodrop and RNA quality was determined using an Agilent 2100 Bioanalyzer. Synthesis and Cy3-labelling of cDNA, and hybridization of the sample to the *B. subtilis*

T3 $2 \times 400\text{K}$ tiling array (Agilent-044473) were performed following Agilent Technologies protocols, as previously described [47]. The microarray was scanned with Agilent Technologies Scanner, model G2505C. Grid: 044473_D_F_20121025. Protocol: GE1_107_Sep09. The tiling array data set is available from NCBI's Gene Expression Omnibus (GEO) database (accession number GSE190460).

2.6. Measurement of dissolved oxygen in the wells

A pO_2 microelectrode (Lazard research laboratories, Inc) was used to measure over time oxygen concentration in the microtiter plate wells. Zero calibration was performed with a 2% sodium bisulfite solution and the results were expressed in ppm.

3. Results

1. Coexistence of submerged biofilms and floating pellicles in microplates wells

In order to confirm that a *B. subtilis* non-domesticated strain was able to grow both as submerged biofilms and floating pellicles in microscopic grade microplate wells, we have combined 4D-CLSM and a long-range objective to monitor both interfacial communities simultaneously. For this, we used a *B. subtilis* NDmed strain derivative constitutively expressing mCherry red fluorescent protein to monitor its growth during 24 h starting from a single layer of adherent cells (Fig. 1, movies S1 and S2 in the supplemental material).

We observed an increase of red fluorescence from the bottom of the well up to a couple of hundred micrometers which corresponds to the development of the submerged biofilm. Increase in fluorescence intensity at the liquid-air interface occurred 7–8 h after the incubation starting point of the adhering cells, corresponding to the formation of the pellicle. It can be seen in Fig. 1 that the distance between the surface and the floating pellicle was initially 4.5 mm, but slightly decreased over time corresponding to liquid evaporation in the well and thereby a consequent drop of the liquid-air interface. Our observations demonstrate that a submerged biofilm and a floating pellicle can form consecutively in the same system. In addition, the fluorescent cells observed in the space between the attached submerged biofilm and the floating pellicles are swimming free cells (see movies S1 and S2), suggesting the existence of an interplay between both communities.

2. A brutal and coordinated fragmentation of sessile elongating chains precede floating pellicle formation

Development of adherent *B. subtilis* NDmed GFP cells on the bottom of the microtiter plates wells was monitored by time-lapse confocal laser scanning microscopy (4D-CLSM) with images taken every 15 min during

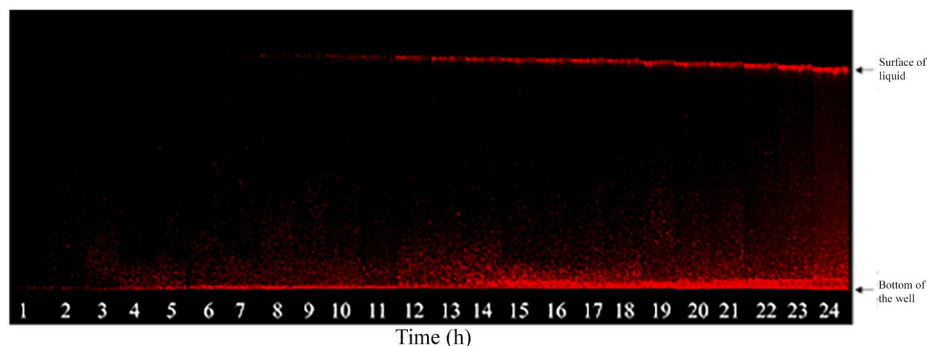


Fig. 1. CLSM Section view of a microplate well colonized by *B. subtilis* NDmed-mCherry showing the relative dynamics of formation of submerged biofilm (bottom of the well) and the floating pellicle (surface of liquid); a representative experiment of three replicates is presented. Note that pellicle slightly falls over time due to liquid evaporation. The distance between the bottom of the well and the surface of the liquid is around 4.5 mm.

14 h (Fig. 2 and movies S3 and S4 in the supplemental material). Fig. 2A represents tile images from the movie S3 at specific time points illustrating the two stages in the surface colonization. In a first stage, sessile cells proliferate as a dense network of long filaments covering the surface. Between 2 and 4 h after they started to proliferate, elongated chains with an average length of around 9 μm suddenly fragment and liberate a cloud of shorter free-swimming cells with an average length of 3 μm (Fig. 2B and C, movie S4). This transition occurred reproducibly in less than 30 min, and the construction of the typical *B. subtilis* protruding structures of sessile cells was visible only in a second kinetic, after 7–9 h (Fig. 2A and B, movie S3).

Similar 4D-CLSM observations were acquired for other *B. subtilis* strains (movies S5-9 in the supplemental material), and strains of other related species (movies S10-12), using the vital FM4-64 fluorescent dye instead of GFP (see details of the strains in Table 1). The reference strains 168 and NCIB3610 displayed a similar behavior to that of the NDmed strain, as well as all other non-domesticated *B. subtilis* isolates tested (NDfood, BsN5 or BSP1). On the contrary, closely related but distinct *Bacillus* species strains such as *Bacillus cereus* 407, *Bacillus licheniformis* LMG7559 or *Bacillus amyloliquefaciens* 20P6 showed a continuous monophasic colonization of the surface without any coordinated liberation of free motile cells (movies S10-12 in the supplemental material).

3. Temporal transcriptome analysis

To understand the mechanism behind sessile cells fragmentation into highly motile ones, a transcriptome analysis by tiling array was done for *B. subtilis* over a temporal scale. A global view of the results indicates that the genes encoding basic functions essential for cellular growth are expressed at a constant rate during the first hours (from 1 h to 7 h), with variation not exceeding at most a factor of 2 (see supplementary data S1). These ensure replication (DNA polymerase, primase, gyrase, topoisomerase, helicase, initiation/termination factors), transcription (RNA polymerase, sigma A factor, elongation/pause/termination factors), translation (ribosomal proteins, aminoacyl-tRNA synthetases, initiation elongation factors) or central carbon metabolism (enzymes of glycolysis and TCA cycle). Thus, this indicates that the process of fragmentation

occurs while cells are growing at a constant rate. Results represented in Fig. S1 confirm the initial microscopic observations, where genes required for autolysis and motility start to be upregulated after 3 h to reach their maximum level after 4 h of incubation, the time in which elongated sessile chains fragment into motile short cells.

Nutrient or/and oxygen depletion were hypothesized to be possible signals triggering the early fragmentation of the sessile chains cells. To investigate the carbon source depletion as a triggering signal, we have monitored expression of *gapB*, a gene encoding a Glycerolaldehyde-3-Phosphate-Dehydrogenase derepressed only under gluconeogenic conditions (supplementary data S1) [48]. The *gapB* gene expression was extremely downregulated during the first 7 h of incubation, and appeared strongly upregulated only in the late samples from 24 h to 48 h, indicating that glycolytic carbon source limitation occurred much later than the fragmentation process.

For oxygen sensing and respiration we have monitored the *hemAT* gene (encoding a soluble chemotaxis receptor oxygen sensor protein) [49], the *cydABCD* operon (encoding cytochrome bd oxidase induced under low oxygen tensions, represented as *cydA* in Fig. S1), and the *qoxABCD* operon (encoding cytochrome *aa3* quinol oxidase, the major oxidase in aerated cultures, represented as *qoxA* gene in Fig. S1) [50]. For efficient aerobic growth, cells require either *CydABCD* or *QoxABCD* [50]. In the first hour only *cydA* appears to be upregulated (Fig. S1) and after 3 h none of the aerobic respiratory genes are expressed. Meanwhile, *hemAT* starts to be upregulated, in synchrony with the fragmentation of sessile cells to motile ones, to reach its maximum expression after 4 h. Aerobic respiration is regained and observed by the upregulation of *qoxA*. Shortly after, anaerobic respiration can be observed (Fig. S1) by upregulation of the self-regulated operon *nark-fnr*, encoding the Fnr transcriptional regulator for anaerobically induced genes, i.e. the *nargHJI* operon and the *arfM* gene encoding another anaerobic regulator. In addition, upregulation is also observed for the *nasBCDEF* operon (represented in Fig. S1 with *nasD* and *nasF*) encoding a nitrate- and a nitrite reductase [51].

Then after 7 h of incubation, biofilm matrix genes (i.e. *epsA*, *tasA*, *dhbA*, *ycvA*, *pgsB*, and *bslA*) are upregulated, the time where the biofilms (submerged and pellicle) are in the process of formation and stabilization. Expression follows of late biofilm genes (i.e. *yxaB*, *veg*, *ymcA*, and

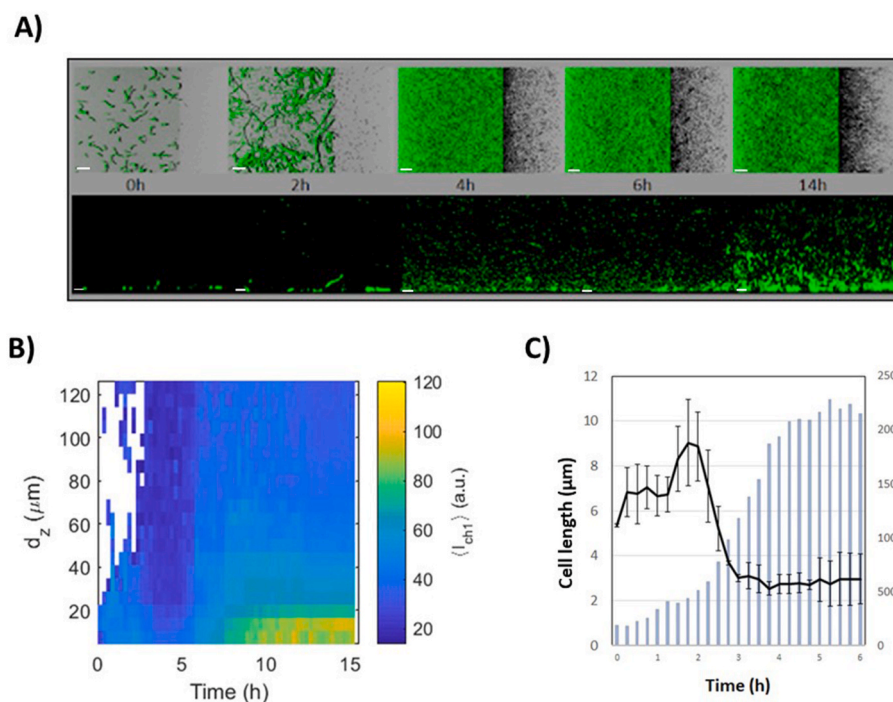


Fig. 2. The biphasic process of submerged biofilm formation by *B. subtilis* NDmed. **A)** 4D-CLSM of *B. subtilis* NDmed GFP on submerged surfaces. Imaris Easy 3D reconstructions (top) and sections views as an XZ projection (bottom) at specific time points of a representative experiment of three independent experiments. The shadow on the right represents a vertical (YZ) projection of the submerged biofilm (scale bars represent 20 μm). **B)** Space-time kymograph generated with BiofilmQ from 4D-CLSM series showing the brutal apparition of free cell in all the well 3h after biofilm initiation and the late initiation of submerged biofilm after 7h. *dz* represents the distance to the surface in μm and *I_{CH1}* the GFP fluorescence intensity in relative arbitrary units. Representative of *n* = 3 independent biofilms. **C)** Individual cell length coordinately and brutally drop during chain fragmentation 2–3 h after biofilm initiation. Chains fragmentation is correlated with an increased number of detected individual objects in the medium. Mean cell length \pm SD calculated from *n* = 3 experiments.

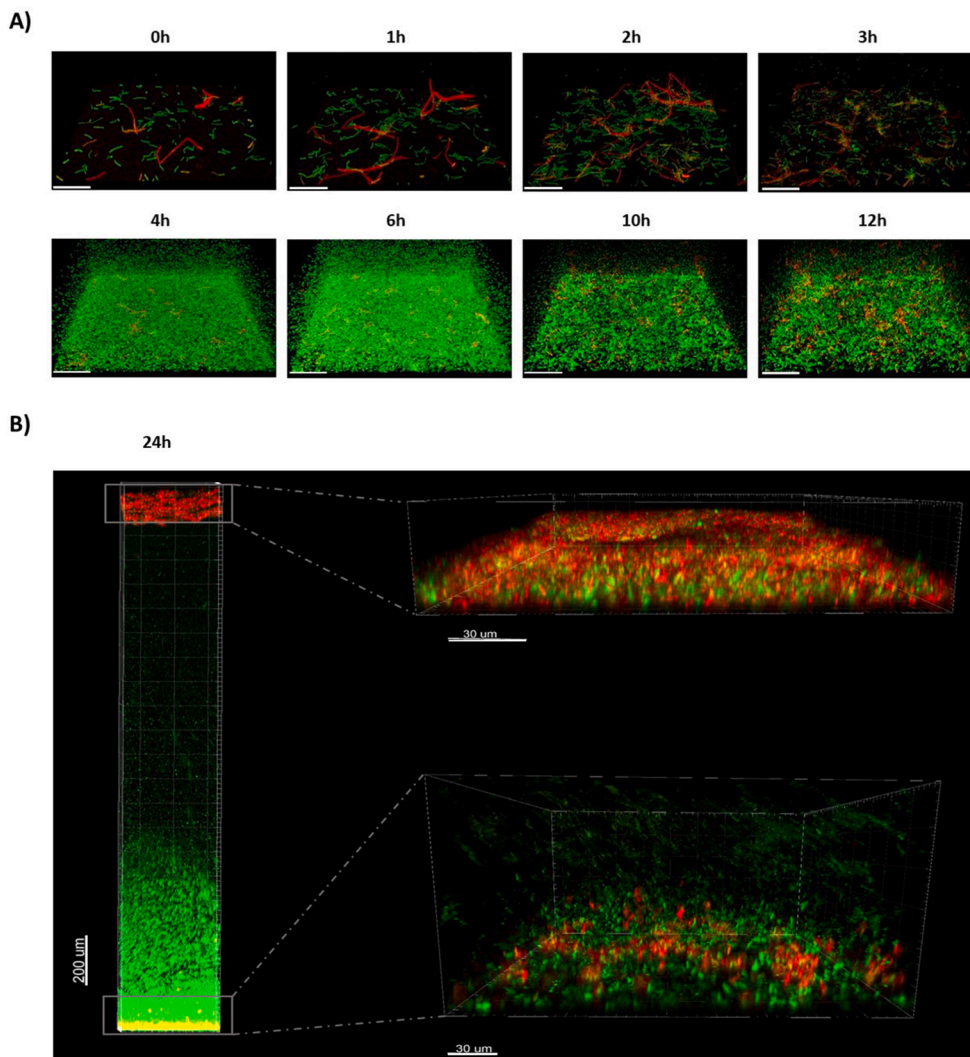


Fig. 3. CLSM of NDmed547 [*amyE::Phag-gfp sacA::PtapA-mKate2*] reporting in green the expression of the *hag* gene (motility) and in red the expression of *tapA* (matrix synthesis). **A)** 4D-CLSM of the biphasic submerged biofilm formation process. See also movie S13. The scale bars represent 50 μm . **B)** CLSM visualization of the well colonization after 24h, both on the surface (with a zoom on submerged biofilm on the bottom right with a scale bar of 30 μm) and at the liquid air interface (with a zoom on a floating pellicle on the up right with a scale bar of 30 μm). (For interpretation of the references to color in this figure legend, the reader is referred to the Web version of this article.)

ypqP) for the complex architectural biofilm formation after 24 and 48 h, as well as genes related to sporulation.

4. *In situ* cell visualization for the fate switching with fluorescent reporters

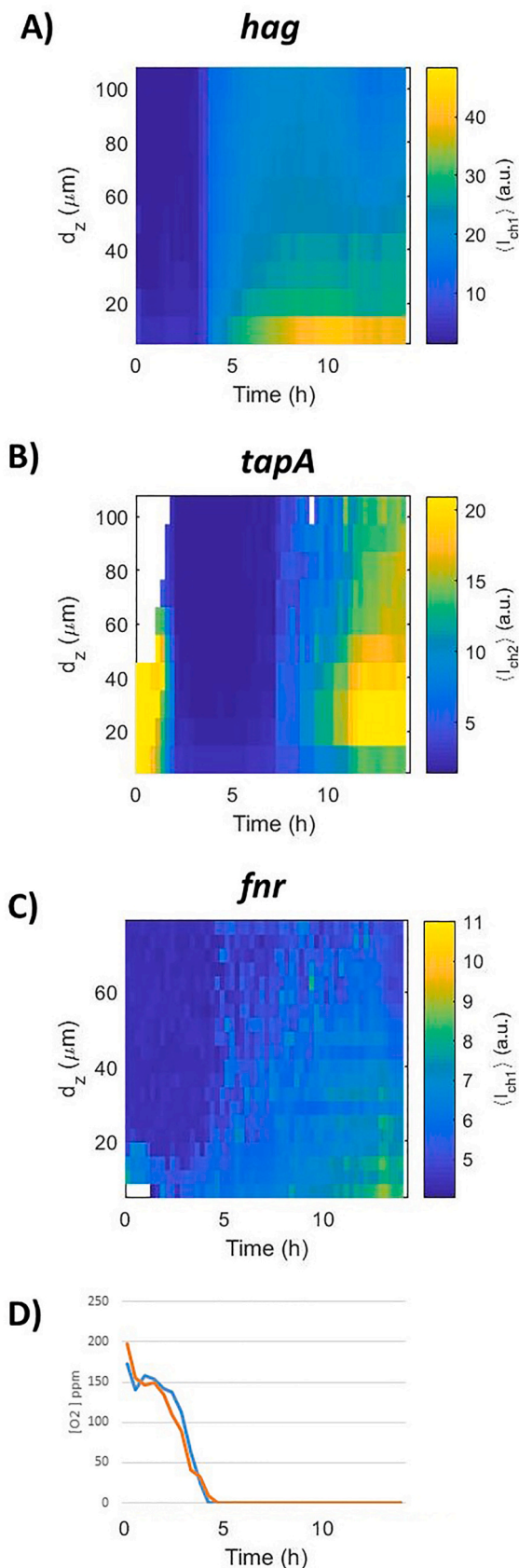
Using the NDmed547 strain harboring two transcriptional reporter constructions, we could monitor both motility and matrix production (*Phag-gfp* reporting the expression of flagella genes in green and *PtapA-mKate2* reporting the expression of matrix genes in red). The submerged biofilm formation was monitored over 14 h (image every 15 min) for the spatio-temporal patterns of these two subpopulations of cell fate (Fig. 3A and movie S13 in the supplementary material). Promoter activities are illustrated in Fig. 4A and B, as a kymograph representing the fluorescence intensity as a function of time and altitude above. Moreover, the GM3361 strain allowed to report in the NDmed context expression of *fnr*, encoding a regulator of the global response to oxygen depletion (*Pfnr-gfpmut3*) (Fig. 4C).

Initially, a subpopulation of sessile chains of cells expressing *tapA* (red) coexists with a subpopulation of motile cells expressing *hag* (green). During the first 3 h of submerged biofilm formation, sessile chains have elongated and propagated, discern visually by the high fluorescent intensity recorded in Fig. 4B, while the fraction of cells expressing *hag* was less abundant (Figs. 3A and 4A). After 3 h, red cell chains (expressing *tapA*) suddenly and coordinately fragment into green

individual motile cells (expressing *hag*), corresponding to the sudden change of the fluorescent intensity color observed in Fig. 4A—a more intense one. In parallel, a clear signal of fluorescence was detectable as early as 3–4 h with GM3361 (*Pfnr-gfpmut3*), indicating that oxygen limitation occurred in early stages of the biofilm development (Fig. 4C). This was confirmed by a direct and continuous measurement of oxygen concentration using a microelectrode (Fig. 4D). Oxygen concentration in the well strictly decreased below the detection limit as early as 4 h after incubation of adherent cells. This oxygen limitation was correlated to trigger the population of red elongated chains, expressing the *tapA* operon, to fragment and acquire motility (Fig. 4). The *tapA* expression was highly regained after ~ 7 h (Fig. S1 and Fig. 4B) to structure the typical surface-associated protruding submerged biofilm and initiate the floating pellicle of *B. subtilis*, which leads to two biofilms in a same well of static liquid culture (Fig. 3B).

4. Discussion

We observed previously that the non-domesticated *B. subtilis* NDmed strain was able to form robust submerged biofilms in the bottom of microtiter-plates under static conditions [28]. In the present work, using 4D-CLSM, we visualized the formation dynamics of these submerged biofilms, which surprisingly appeared to be a discontinuous process. After a first stage of development on the surface, and concomitantly with oxygen limitation, sessile chains suddenly fragment, liberating a



(caption on next column)

Fig. 4. Space-time kymographs for reporters (A) *hag*, (B) *tapA*, (C) *fnr* transcription during submerged biofilm formation of *B. subtilis* NDmed. Representative of $n = 3$ independent biofilms for each reporter. Kymographs were constructed with BiofilmQ visualization toolbox from 4D-CLSM image sequences with fluorescent transcriptional fusions (NDmed547 [*amyE::Phag-gfp sacA::PtapA-mKate2*] and GM3361 [*Pfnr-gfpmut3*]). d_z represents the distance to the surface in μm and I_{ch1} the fluorescent reporter intensity in relative arbitrary units. The graph in panel (D) represents the oxygen concentration measured in two wells with a microelectrode showing a sharp decrease of oxygen concentration that drops from around 185 ppm at $t = 0$ below the probe detection limit after less than 5 h.

massive number of free motile cells. These planktonic cells partially migrate towards the liquid-air interface to initiate a floating pellicle. It is only in a second kinetics that the characteristic surface-associated protruding structures of *B. subtilis* NDmed rise, along with strong expression of the *tapA-sipW-tasA* matrix operon. To our knowledge, such biphasic biofilm formation has never been explored and when pellicles and submerged biofilms have been studied, it was frequently under different conditions.

In other bacterial species like *Pseudomonas aeruginosa*, detachment from the surface and dispersion has been described as a possible end to the biofilm lifestyle cycle. The active cells scattering from biofilm to new habitats seem to be driven by limitations of resources or the emergence of stressful conditions in the cell microenvironment. Depletion in nutrient availability or the accumulation of waste metabolic products (such as acids issuing from fermentation in oxygen-depleted zones) have been demonstrated to induce biofilm dispersal [52]. In the work presented here, we demonstrate that early oxygen limitation in the well is concomitant with massive liberation of planktonic cells from early submerged biofilm after approximately 4 h of development. In *B. subtilis*, oxygen depletion has been shown previously to induce matrix production by increasing transcription of the *tapA* operon in NCIB3610 colonies [53]. In our submerged system, expression in NDmed of *tapA* was also correlated with that of *fnr*, a gene induced under deep oxygen depletion. These observations suggest that, after a first step of proliferation of sessile cells as filaments covering the surface, the limitation of oxygen triggered their fragmentation into motile cells able to migrate to the air-medium interface to form the pellicle. Indeed, a temporal transcriptome analysis of biofilm showed that genes involved in oxygen sensing, autolysis and motility were highly expressed after 4 h of development, which corresponded to the sudden transition between filaments and motile cells observed with 4D-CLSM. This is in accordance with a previous report identifying oxygen as a putative trigger for active movement towards the air-liquid interface of *B. subtilis* NCIB3610 cells, since a $\Delta hemAT$ mutant was outcompeted by the wild type during pellicle formation in static co-cultures [54]. Similar behaviors were also described for the Gram-negative lake sediment bacterium *Shewanella oneidensis* MR-1, as biofilms formed by this species showed a rapid detachment from the surface upon a sudden downshift in oxygen concentration [55].

Interestingly, all other *B. subtilis* strains tested, including thick biofilm-forming isolates such as NDfood, BsN5 and BsP1, or weaker submerged biofilm-forming strains 168 and NCIB3610, showed a similar biphasic submerged biofilm dynamics (Movies S5-9). In contrast, other related species, such as *B. cereus*, *B. amyloliquefaciens* or *B. licheniformis* exhibited a continuous colonization of the surface (Movies S10-12). Some of these *Bacilli* are also able to form chains of cells, but which did not fragment during the time the biofilm formation was monitored. *B. subtilis* chain formation was first visualized in pellicles [11], however without observation of coordinated return to planktonic state in these conditions. The relation between submerged biofilm and liquid-air pellicle shown here could suggest an interplay, with co-metabolism between the populations of both interfaces: the population in contact with air could liberate metabolites used by the surface-associated population to grow in anaerobic condition. This is consistent with the

described ability of *B. subtilis* to grow without oxygen, respiring nitrate or nitrite instead of oxygen as electrons acceptor [56]. Nevertheless, this potential relation between populations requires further investigation.

Understanding the triggers and effectors of this coordinated multicellular behavior could also contribute to identifying new actors involved in biofilm disruption. This has been largely studied in recent years because of its potential as an alternative treatment to promote biofilm cell detachment [57,58]. Some natural molecules produced by mature biofilms have been found to induce biofilm disassembly, such as nitric oxide in *Pseudomonas* spp. biofilms [59] or acidic amino acids in *S. aureus* biofilms [60]. The combination of such biofilm disruptors with antibiotics treatment to improve drug effectiveness could be a promising approach to tackle biofilm chronic infections.

The experimental approach proposed in this work allowed visualization, at the cell level, of the dynamic interactions between subpopulations in a *B. subtilis* community. The multidimensional description of spatio-temporal patterns of gene expression has been recently facilitated by the availability to biologists of advanced quantitative microscopic analysis tools [44]. The implementation of this system to more complex samples, such as multispecies biofilms, could provide an experimental approach for the study of spatial interactions between species, co-metabolism or cell-to-cell signaling.

CRedit authorship contribution statement

Pilar Sanchez-Vizuete: Conceptualization, experiments, Writing – original draft. **Yasmine Dergham:** Conceptualization, experiments, Data curation, Writing – original draft, Writing – review & editing. **Arnaud Bridier:** Conceptualization, experiments, Writing – review & editing. **Julien Deschamps:** Assistance with 4D-CLSM microscopy, Formal analysis. **Etienne Dervyn:** Transcriptomic experiments. **Kassem Hamze:** Supervision, reviewing. **Stéphane Aymerich:** Conceptualization, reviewing. **Dominique Le Coq:** Conceptualization, Methodology, Supervision, Writing – review & editing. **Romain Briandet:** Conceptualization, Methodology, Supervision, Writing – review & editing.

Declaration of competing interest

The authors declare that they have no known competing financial interests or personal relationships that could have appeared to influence the work reported in this paper.

Acknowledgments

This work was supported by INRAE. P. Sanchez-Vizuete was the recipient of a PhD grant from the Région Ile-de-France (DIM ASTREA). Y. Dergham is the recipient of fundings from the Union of Southern Suburbs Municipalities of Beirut, INRAE, Campus France PHC CEDRE 42280 PF and Fondation AgroParisTech. L. Tournier and V. Fromion (INRAE) are acknowledged for fruitful discussions, R. Losick for the gift of the strain TMN547, and M. Jules for the gift of strains BBA0184 and BBA9006.

Appendix A. Supplementary data

Supplementary data to this article can be found online at <https://doi.org/10.1016/j.biofilm.2021.100065>.

References

- [1] Karygianni L, Ren Z, Koo H, Thurnheer T. Biofilm matrixome: extracellular components in structured microbial communities. *Trends Microbiol* 2020;28:668–81. <https://doi.org/10.1016/j.tim.2020.03.016>.
- [2] Flemming H-C, Wingender J, Szewzyk U, Steinberg P, Rice SA, Kjelleberg S. Biofilms: an emergent form of bacterial life. *Nat Rev Microbiol* 2016;14:563–75. <https://doi.org/10.1038/nrmicro.2016.94>.
- [3] Mukherjee M, Cao B. Engineering controllable biofilms for biotechnological applications. *Microb Biotechnol* 2021;14:74–8. <https://doi.org/10.1111/1751-7915.13715>.
- [4] Mah T-F. Biofilm-specific antibiotic resistance. *Future Microbiol* 2012;7:1061–72. <https://doi.org/10.2217/fmb.12.76>.
- [5] Nickel JC, Ruseska I, Wright JB, Costerton JW. Tobramycin resistance of *Pseudomonas aeruginosa* cells growing as a biofilm on urinary catheter material. *Antimicrob Agents Chemother* 1985;27:619–24. <https://doi.org/10.1128/AAC.27.4.619>.
- [6] Costerton JW, Stewart PS, Greenberg EP. Bacterial biofilms: a common cause of persistent infections. *Science* 1999;284:1318–22. <https://doi.org/10.1126/science.284.5418.1318>.
- [7] da Silva RAG, Afonina I, Kline KA. Eradicating biofilm infections: an update on current and prospective approaches. *Curr Opin Microbiol* 2021;63:117–25. <https://doi.org/10.1016/j.mib.2021.07.001>.
- [8] Pamp SJ, Sternberg C, Tolker-Nielsen T. Insight into the microbial multicellular lifestyle via flow-cell technology and confocal microscopy. *Cytometry A* 2009;75:90–103. <https://doi.org/10.1002/cyto.a.20685>.
- [9] Branda SS, González-Pastor JE, Ben-Yehuda S, Losick R, Kolter R. Fruiting body formation by *Bacillus subtilis*. *Proc Natl Acad Sci U S A* 2001;98:11621–6. <https://doi.org/10.1073/pnas.191384198>.
- [10] Piggot PJ, Hilbert DW. Sporulation of *Bacillus subtilis*. *Curr Opin Microbiol* 2004;7:579–86. <https://doi.org/10.1016/j.mib.2004.10.001>.
- [11] Kobayashi K. *Bacillus subtilis* pellicle formation proceeds through genetically defined morphological changes. *J Bacteriol* 2007;189:4920–31. <https://doi.org/10.1128/JB.00157-07>.
- [12] Vlamakis H, Chai Y, Beauregard P, Losick R, Kolter R. Sticking together: building a biofilm the *Bacillus subtilis* way. *Nat Rev Microbiol* 2013;11:157–68. <https://doi.org/10.1038/nrmicro2960>.
- [13] Sanchez-Vizuete P, Le Coq D, Bridier A, Herry J-M, Aymerich S, Briandet R. Identification of *yppQ* as a New *Bacillus subtilis* biofilm determinant that mediates the protection of *Staphylococcus aureus* against antimicrobial agents in mixed-species communities. *Appl Environ Microbiol* 2015;81:109–18. <https://doi.org/10.1128/AEM.02473-14>.
- [14] Kearns DB, Chu F, Branda SS, Kolter R, Losick R. A master regulator for biofilm formation by *Bacillus subtilis*. *Mol Microbiol* 2005;55:739–49. <https://doi.org/10.1111/j.1365-2958.2004.04440.x>.
- [15] Cairns LS, Hobbly L, Stanley-Wall NR. Biofilm formation by *Bacillus subtilis*: new insights into regulatory strategies and assembly mechanisms. *Mol Microbiol* 2014;93:587–98. <https://doi.org/10.1111/mmi.12697>.
- [16] Bartolini M, Cogliati S, Vileta D, Bauman C, Rateni L, Leñini C, et al. Regulation of biofilm aging and dispersal in *Bacillus subtilis* by the alternative sigma factor SigB. *J Bacteriol* 2019;201. <https://doi.org/10.1128/JB.00473-18>. e00473-18.
- [17] Milton ME, Draughn GL, Bobay BG, Stowe SD, Olson AL, Feldmann EA, et al. The solution structures and interaction of SinR and SinI: elucidating the mechanism of action of the master regulator switch for biofilm formation in *Bacillus subtilis*. *J Mol Biol* 2020;432:343–57. <https://doi.org/10.1016/j.jmb.2019.08.019>.
- [18] Nishikawa M, Kobayashi K. Calcium prevents biofilm dispersion in *Bacillus subtilis*. *J Bacteriol* 2021;203:e0011421. <https://doi.org/10.1128/JB.00114-21>.
- [19] Arnaouteli S, Bamford NC, Stanley-Wall NR, Kovács ÁT. *Bacillus subtilis* biofilm formation and social interactions. *Nat Rev Microbiol* 2021. <https://doi.org/10.1038/s41579-021-00540-9>.
- [20] Chai Y, Kolter R, Losick R. Reversal of an epigenetic switch governing cell chaining in *Bacillus subtilis* by protein instability. *Mol Microbiol* 2010;78:218–29. <https://doi.org/10.1111/j.1365-2958.2010.07335.x>.
- [21] López D, Kolter R. Extracellular signals that define distinct and coexisting cell fates in *Bacillus subtilis*. *FEMS Microbiol Rev* 2010;34:134–49. <https://doi.org/10.1111/j.1574-6976.2009.00199.x>.
- [22] Diethmaier C, Pietack N, Gunka K, Wrede C, Lehn-Habrink M, Herzberg C, et al. A novel factor controlling bistability in *Bacillus subtilis*: the YmdB protein affects flagellin expression and biofilm formation. *J Bacteriol* 2011;193:5997–6007. <https://doi.org/10.1128/JB.05360-11>.
- [23] Romero D, Aguilar C, Losick R, Kolter R. Amyloid fibers provide structural integrity to *Bacillus subtilis* biofilms. *Proc Natl Acad Sci U S A* 2010;107:2230–4. <https://doi.org/10.1073/pnas.0910560107>.
- [24] Ostrowski A, Mehert A, Prescott A, Kiley TB, Stanley-Wall NR. YuaB functions synergistically with the exopolysaccharide and TasA amyloid fibers to allow biofilm formation by *Bacillus subtilis*. *J Bacteriol* 2011;193:4821–31. <https://doi.org/10.1128/JB.00223-11>.
- [25] Kobayashi K, Iwano M. BslA(YuaB) forms a hydrophobic layer on the surface of *Bacillus subtilis* biofilms. *Mol Microbiol* 2012;85:51–66. <https://doi.org/10.1111/j.1365-2958.2012.08094.x>.
- [26] Roux D, Cywes-Bentley C, Zhang Y-F, Pons S, Konkol M, Kearns DB, et al. Identification of poly-N-acetylglucosamine as a major polysaccharide component of the *Bacillus subtilis* biofilm matrix. *J Biol Chem* 2015;290:19261–72. <https://doi.org/10.1074/jbc.M115.648709>.
- [27] El Mammeri N, Hierrezuelo J, Tolchard J, Cámara-Almirón J, Caro-Astorga J, Álvarez-Mena A, et al. Molecular architecture of bacterial amyloids in *Bacillus* biofilms. *FASEB J* 2019;33:12146–63. <https://doi.org/10.1096/fj.201900831R>.
- [28] Bridier A, Le Coq D, Dubois-Brissonnet F, Thomas V, Aymerich S, Briandet R. The spatial architecture of *Bacillus subtilis* biofilms deciphered using a surface-associated model and in situ imaging. *PLoS One* 2011;6:e16177. <https://doi.org/10.1371/journal.pone.0016177>.
- [29] Bridier A, Sanchez-Vizuete MDP, Le Coq D, Aymerich S, Meylheuc T, Maillard J-Y, et al. Biofilms of a *Bacillus subtilis* hospital isolate protect *Staphylococcus aureus*

- from biocide action. *PLoS One* 2012;7:e44506. <https://doi.org/10.1371/journal.pone.0044506>.
- [30] Abe K, Kawano Y, Iwamoto K, Arai K, Maruyama Y, Eichenberger P, et al. Developmentally-regulated excision of the SPβ prophage reconstitutes a gene required for spore envelope maturation in *Bacillus subtilis*. *PLoS Genet* 2014;10:e1004636. <https://doi.org/10.1371/journal.pgen.1004636>.
- [31] Chen Y, Yan F, Chai Y, Liu H, Kolter R, Losick R, et al. Biocontrol of tomato wilt disease by *Bacillus subtilis* isolates from natural environments depends on conserved genes mediating biofilm formation. *Environ Microbiol* 2013;15:848–64. <https://doi.org/10.1111/j.1462-2920.2012.02860.x>.
- [32] Pandin C, Le Coq D, Canette A, Aymerich S, Briandet R. Should the biofilm mode of life be taken into consideration for microbial biocontrol agents? *Microb Biotechnol* 2017;10:719–34. <https://doi.org/10.1111/1751-7915.12693>.
- [33] Terra R, Stanley-Wall NR, Cao G, Lazazzera BA. Identification of *Bacillus subtilis* SipW as a bifunctional signal peptidase that controls surface-adhered biofilm formation. *J Bacteriol* 2012;194:2781–90. <https://doi.org/10.1128/JB.06780-11>.
- [34] Dergham Y, Sanchez-Vizuete P, Le Coq D, Deschamps J, Bridier A, Hamze K, et al. Comparison of the genetic features involved in *Bacillus subtilis* biofilm formation using multi-culturing approaches. *Microorganisms* 2021;9:633. <https://doi.org/10.3390/microorganisms9030633>.
- [35] Martin DJH, Denyer SP, McDonnell G, Maillard J-Y. Resistance and cross-resistance to oxidising agents of bacterial isolates from endoscope washer disinfectors. *J Hosp Infect* 2008;69:377–83. <https://doi.org/10.1016/j.jhin.2008.04.010>.
- [36] Norman TM, Lord ND, Paulsson J, Losick R. Memory and modularity in cell-fate decision making. *Nature* 2013;503:481–6. <https://doi.org/10.1038/nature12804>.
- [37] Rühl M, Le Coq D, Aymerich S, Sauer U. 13C-flux analysis reveals NADPH-balancing transhydrogenation cycles in stationary phase of nitrogen-starving *Bacillus subtilis*. *Journal of Biological Chemistry* 2012;287:27959–70. <https://doi.org/10.1074/jbc.M112.366492>.
- [38] Botella E, Fogg M, Jules M, Piersma S, Doherty G, Hansen A, et al. pBaSysBioII: an integrative plasmid generating gfp transcriptional fusions for high-throughput analysis of gene expression in *Bacillus subtilis*. *Microbiology (Reading)* 2010;156:1600–8. <https://doi.org/10.1099/mic.0.035758-0>.
- [39] Deng Y, Zhu Y, Wang P, Zhu L, Zheng J, Li R, et al. Complete genome sequence of *Bacillus subtilis* BSn5, an endophytic bacterium of *Amorphophallus konjac* with antimicrobial activity for the plant pathogen *Erwinia carotovora* subsp. *carotovora*. *J Bacteriol* 2011;193:2070–1. <https://doi.org/10.1128/JB.00129-11>.
- [40] Schyns G, Serra CR, Lapointe T, Pereira-Leal JB, Potot S, Fickers P, et al. Genome of a gut strain of *Bacillus subtilis*. *Genome Announc* 2013;1. <https://doi.org/10.1128/genomeA.00184-12>. e00184-12.
- [41] Houry A, Briandet R, Aymerich S, Gohar M. Involvement of motility and flagella in *Bacillus cereus* biofilm formation. *Microbiology (Reading)* 2010;156:1009–18. <https://doi.org/10.1099/mic.0.034827-0>.
- [42] De Clerck E, De Vos P. Genotypic diversity among *Bacillus licheniformis* strains from various sources. *FEMS Microbiol Lett* 2004;231:91–8. [https://doi.org/10.1016/S0378-1097\(03\)00935-2](https://doi.org/10.1016/S0378-1097(03)00935-2).
- [43] Bridier A, Dubois-Brissonnet F, Boubetra A, Thomas V, Briandet R. The biofilm architecture of sixty opportunistic pathogens deciphered using a high-throughput CLSM method. *J Microbiol Methods* 2010;82:64–70. <https://doi.org/10.1016/j.mimet.2010.04.006>.
- [44] Hartmann R, Jeckel H, Jelli E, Singh PK, Vaidya S, Bayer M, et al. Quantitative image analysis of microbial communities with BiofilmQ. *Nat Microbiol* 2021;6:151–6. <https://doi.org/10.1038/s41564-020-00817-4>.
- [45] Ayachit U. "The ParaView guide: a parallel visualization application," in. 2015. Clifton Park, USA: Kitware.
- [46] Nicolas P, Mäder U, Dervyn E, Rochat T, Leduc A, Pigeonneau N, et al. Condition-dependent transcriptome reveals high-level regulatory architecture in *Bacillus subtilis*. *Science* 2012;335:1103–6. <https://doi.org/10.1126/science.1206848>.
- [47] Rath H, Sappa PK, Hoffmann T, Salazar MG, Reder A, Steil L, et al. Impact of high salinity and the compatible solute glycine betaine on gene expression of *Bacillus subtilis*. *Environ Microbiol* 2020;22:3266–86. <https://doi.org/10.1111/1462-2920.15087>.
- [48] Fillinger S, Boschi-Muller S, Azza S, Dervyn E, Branlant G, Aymerich S. Two glyceraldehyde-3-phosphate dehydrogenases with opposite physiological roles in a nonphotosynthetic bacterium. *J Biol Chem* 2000;275:14031–7. <https://doi.org/10.1074/jbc.275.19.14031>.
- [49] Hou S, Larsen RW, Boudko D, Riley CW, Karatan E, Zimmer M, et al. Myoglobin-like aerotaxis transducers in archaea and bacteria. *Nature* 2000;403:540–4. <https://doi.org/10.1038/35000570>.
- [50] Sachla AJ, Luo Y, Helmann JD. Manganese impairs the QoxABCD terminal oxidase leading to respiration-associated toxicity. *Mol Microbiol* 2021. <https://doi.org/10.1111/mmi.14767>.
- [51] Nakano MM, Zuber P. Anaerobic growth of a "strict aerobe" (*Bacillus subtilis*). *Annu Rev Microbiol* 1998;52:165–90. <https://doi.org/10.1146/annurev.micro.52.1.165>.
- [52] Rumbaugh KP, Sauer K. Biofilm dispersion. *Nat Rev Microbiol* 2020;18:571–86. <https://doi.org/10.1038/s41579-020-0385-0>.
- [53] Kolodkin-Gal I, Elsholz AKW, Muth C, Girguis PR, Kolter R, Losick R. Respiration control of multicellularity in *Bacillus subtilis* by a complex of the cytochrome chain with a membrane-embedded histidine kinase. *Genes Dev* 2013;27:887–99. <https://doi.org/10.1101/gad.215244.113>.
- [54] Hölscher T, Bartels B, Lin Y-C, Gallegos-Monterrosa R, Price-Whelan A, Kolter R, et al. Motility, chemotaxis and aerotaxis contribute to competitiveness during bacterial pellicle biofilm development. *J Mol Biol* 2015;427:3695–708. <https://doi.org/10.1016/j.jmb.2015.06.014>.
- [55] Thormann KM, Saville RM, Shukla S, Spormann AM. Induction of rapid detachment in *Shewanella oneidensis* MR-1 biofilms. *J Bacteriol* 2005;187:1014–21. <https://doi.org/10.1128/JB.187.3.1014-1021.2005>.
- [56] Nakano MM, Hulett FM. Adaptation of *Bacillus subtilis* to oxygen limitation. *FEMS Microbiol Lett* 1997;157:1–7. <https://doi.org/10.1111/j.1574-6968.1997.tb12744.x>.
- [57] Kostakioti M, Hadjifrangiskou M, Hultgren SJ. Bacterial biofilms: development, dispersal, and therapeutic strategies in the dawn of the postantibiotic era. *Cold Spring Harb Perspect Med* 2013;3:a010306. <https://doi.org/10.1101/cshperspect.a010306>.
- [58] Cascioferro S, Carbone D, Parrino B, Pecoraro C, Giovannetti E, Cirrincione G, et al. Therapeutic strategies to counteract antibiotic resistance in MRSA biofilm-associated infections. *ChemMedChem* 2021;16:65–80. <https://doi.org/10.1002/cmdc.202000677>.
- [59] Barraud N, Kelso MJ, Rice SA, Kjelleberg S. Nitric oxide: a key mediator of biofilm dispersal with applications in infectious diseases. *Curr Pharm Des* 2015;21:31–42. <https://doi.org/10.2174/1381612820666140905112822>.
- [60] Warrach AA, Mohammed AR, Perrie Y, Hussain M, Gibson H, Rahman A. Evaluation of anti-biofilm activity of acidic amino acids and synergy with ciprofloxacin on *Staphylococcus aureus* biofilms. *Sci Rep* 2020;10:9021. <https://doi.org/10.1038/s41598-020-66082-x>.